



HAL
open science

Sodium nanoparticles in alkali halide minerals: Why is villiaumite red and halite blue?

Georges Calas, Laurence Galois, Alexis Geisler

► To cite this version:

Georges Calas, Laurence Galois, Alexis Geisler. Sodium nanoparticles in alkali halide minerals: Why is villiaumite red and halite blue?. *The American Mineralogist*, 2021, 106 (5), pp.838-842. 10.2138/am-2021-7917 . hal-03236416

HAL Id: hal-03236416

<https://hal.sorbonne-universite.fr/hal-03236416>

Submitted on 26 May 2021

HAL is a multi-disciplinary open access archive for the deposit and dissemination of scientific research documents, whether they are published or not. The documents may come from teaching and research institutions in France or abroad, or from public or private research centers.

L'archive ouverte pluridisciplinaire **HAL**, est destinée au dépôt et à la diffusion de documents scientifiques de niveau recherche, publiés ou non, émanant des établissements d'enseignement et de recherche français ou étrangers, des laboratoires publics ou privés.

1 **REVISION 1**

2
3 **SODIUM NANOPARTICLES IN ALKALI HALIDE MINERALS:**

4 **WHY IS VILLIAUMITE RED AND HALITE BLUE?**

5
6 Georges Calas ^a, Laurence Galois ^a and Alexis Geisler ^a

7
8 ^a *Sorbonne Université, Muséum National d'Histoire Naturelle, CNRS, Institut de Minéralogie,*
9 *de Physique des Matériaux et de Cosmochimie, IMPMC, 75005 Paris, France*

10 **corresponding author : Georges Calas, Sorbonne Université, IMPMC, BC 115, 4 place*
11 *Jussieu 75005 Paris, France. georges.calas@sorbonne-universite.fr*

12
13
14 **ABSTRACT**

15 The presence of metal Na nanoparticles causes the bright, thermally unstable colors of
16 villiaumite, NaF, and halite, NaCl. These nanoparticles have been suspected since a long time to
17 be caused by external irradiation. Metal nanoparticles, often referred to as metal colloids, cause
18 surface plasmon resonance effects, characterized by a single Lorentzian-shaped absorption band.
19 The color of these minerals is due to metal Na nanoparticles of 2.5-3 nm. A key point is that the
20 resonance wavelength, which corresponds to the maximum of the absorption band, is inversely
21 related to the value of the refractive index of the embedding mineral. This causes the position of
22 the main absorption band to be offset downwards by 140 nm in halite relative to villiaumite. As a
23 consequence, the optical transmission window is shifted from the long to the short wavelength
24 domain, explaining the color of blue halite and red villiaumite, respectively. Similar refractive

25 index dependence may explain the purple color of fluorite, caused by metallic Ca nanoparticles.
26 Finally, the origin of the villiaumite irradiation may be the presence of Th-rich (about 8.8wt%
27 ThO₂) nano-inclusions, about 500 nm large, illustrating the specific geochemistry of peralkaline
28 rocks where villiaumite is found.

29

30 **Keywords:** villiaumite, halite, fluorite, peralkaline rocks, color, radiation damage, UV-visible
31 spectroscopy, nanoparticles

32

33

INTRODUCTION

34 One of the outstanding properties of alkali halides is their optical transparency from the
35 vacuum UV to the far infrared. Though they are intrinsically colorless, they sometimes show a
36 thermally unstable coloration, which, in the absence of chemical impurities, has long been
37 recognized to result from radiation damage (e.g., Prizibram, 1953; Stormer and Carmichael, 1970).
38 The simplest radiation-induced defect is the so-called F center, i.e. an electron trapped in an
39 anion vacancy. The F center creates a singly occupied electronic level in the band gap, which
40 colors the crystal. The aggregation of two or three F centers on nearest neighbor sites, gives rise
41 to binary M- and ternary R-centers, respectively. Eventually, color centers aggregate to form
42 metallic alkali nanoparticles, also referred to as colloids, caused by an irradiation at room
43 temperature or higher temperatures (see e.g., Schwartz et al., 2008). Optical properties of metal
44 nanoparticles have unique characteristics that give rise to brilliant colors. For instance, during
45 external irradiation of synthetic halite, the change from a yellow color due to *F*-centers to a bright
46 blue color indicates the formation of Na metal nanoparticles (Kreibig and Vollmer, 1995).

47 Natural halite, NaCl, presents various radiation-induced colors (Zepek et al., 2015), but blue
48 hues with a broad range of saturation are the most frequent (Supplemental Figure 1). The blue
49 color has been assigned to colloidal Na metal formed by irradiation with ionizing radiation
50 (Rossman, 2010). Radiation defects in halite provide information on the sedimentary history of
51 salt deposits (Sonnenfeld, 1995; Zepek et al., 2014 and 2015) or the stability of nuclear waste
52 repositories (Levy et al., 1983). Recently, they have been used to assess the exposure duration of
53 the surface of icy moons (Poston et al., 2017) and ordinary chondrites (Chan et al., 2018), subject
54 to cosmic radiation. Villiaumite, NaF, is an accessory phase formed during a late pegmatitic stage
55 associated with peralkaline nepheline syenites (Stormer and Carmichael, 1970; Marks and Markl,
56 2017). It is generally characterized by its intense carmine red color (Supplemental Figure S2).

57 The origin of the red color of natural villiaumite has not yet been investigated, though it is
58 suspected to arise from radiation damage (Rossman, 2010). By contrast, blue halite received
59 much attention, with pioneering studies on samples from Strassfurt, Germany (Przibram, 1953;
60 Doyle, 1960; Howard and Kerr, 1960; Arun et al., 2017) and, more recently, Kłodawa, Poland
61 (Weselucha-Birczynska et al., 2012; Zepek et al., 2014 and 2015) and Morleben, Germany (Arun et
62 al., 2017) salt mines. This study shows that the red color of villiaumite is a result of a surface
63 plasmon resonance (Kreibig and Vollmer, 1995) due to Na metal nanoparticles. The optical
64 spectra of blue halite have a similar origin. The outstanding color change between blue halite and
65 red villiaumite is rationalized in terms of the dependence of the wavelength resonance of the
66 nanoparticles on the refractive index of the embedding mineral. The same formalism may be
67 extended to explain the origin of the purple color of fluorite, due to the presence of calcium
68 metallic nanoparticles. The origin of the villiaumite irradiation may be the presence of Th-rich
69 (about 8.8wt% ThO₂) nano-inclusions, about 500 nm large, illustrating the geochemistry of
70 peralkaline rocks where villiaumite is found.

71

72

MATERIALS AND METHODS

73 Villiaumite crystals come from the agpaitic suite of nepheline syenites of the type locality of
74 the Los Archipelago, Guinea (Lacroix, 1908; Moreau et al., 1998). A sedimentary navy blue
75 halite from Strassfurt (Germany) was used for comparison. Optical absorption spectra were
76 measured at room temperature and at 10K in the spectral range 200–3300 nm ($50,000\text{ cm}^{-1}$ - $3,030$
77 cm^{-1}), using a double-beam computerized Perkin-Elmer Lambda 1050 UV–Visible-NIR
78 spectrophotometer. The spectral resolution varies from 0.8 nm in the UV region to 2 nm in the
79 near IR - visible region. A He-cryostat under vacuum (around 3.4×10^{-7} mbar) was used to
80 record spectra at 10 K. The optical absorption spectra were obtained in transmission mode on
81 cleaved crystals (Supplemental Figure S3). The spectra were normalized to sample thickness and
82 background corrected using a polynomial function. The data are presented and analyzed as a
83 function of wavelength, as the absorption is caused by surface plasmon resonance effects
84 interpreted in terms of the Mie theory (see e.g., Kreibig and Vollmer, 1995). Preliminary
85 scanning electron microscopy with field emission gun (SEM-FEG) analyses were obtained at 15
86 kV and a beam current of 200 nA with a Zeiss Ultra 55 instrument fitted with a high-resolution
87 Schottky FEG and a UHR Gemini® column. Semi-quantitative analyses were performed using a
88 Bruker Quantax XFlash 4010 energy-dispersive X-ray spectrometer.

89

90

RESULTS AND DISCUSSION

Optical absorption spectra of villiaumite

92 The samples investigated present an intense red color, which disappears in a couple of minutes
93 at 500 °C and after 2 hrs at 400°C. The room temperature optical absorption spectrum
94 (Supplemental Figure S4) shows the presence of a background due to light scattering by

95 inclusions and fractures that result from the easy {100} cleavage of this cubic mineral. After
96 subtracting this background contribution, the most salient feature is an intense absorption band at
97 494 nm. The two other contributions are a shoulder near 415 nm and a small band at 328 nm
98 (Figure 1a). This spectrum is similar to the one of villiaumite from Mont Saint Hilaire, Canada
99 (Rossman, 2010), which is dominated by a main absorption band peaking at 510 nm.

100 The optical absorption spectra have been fitted using a minimum of components, chosen to
101 correspond to spectroscopic events. Gaussian and Lorentzian lineshapes of the spectral
102 components have been tested. Indeed, by contrast to the Gaussian shape of absorption bands
103 caused by color centers (see e.g. Jenkins et al., 2000; Hoya et al., 2017), surface plasmon
104 resonances exhibited by metallic nanoparticles give rise to Lorentzian-shaped absorption bands,
105 as predicted by Mie theory (Kreibig and Vollmer, 1995; Seinen et al., 1994; Ruiz-Fuertes et al.,
106 2019). A good fit of the main band is achieved by using a Lorentzian function peaking at 494 nm.
107 The full width at half-maximum (FWHM) of this band, 86 nm, is larger than that of the other
108 contributions due to color centers. This Lorentzian lineshape explains the presence of a long tail
109 extending towards long wavelengths, at the origin of the intense red hue of villiaumite. Such a
110 Lorentzian line-shape characterizes the optical spectra of free neutral Na clusters (Selby et al.,
111 1991), Na nanoparticles in NaCl (Seinen et al., 1994) and NaF (Seifert et al., 1994) or Ca
112 nanoparticles in CaF₂ (Ruiz- Fuertes et al., 2019; Ryskin et al., 2020).

113 The two minor contributions at 328 nm and 414 nm have a Gaussian lineshape. The former
114 corresponds to a *F*-center, widely investigated in synthetic NaF (Seifert et al., 1994; Tiwald et al.,
115 2015; Hoya et al., 2017). The latter may be assigned to a *R*-center (Amenu-Kpodo and Neubert,
116 1965; Bryukvina and Martynovich, 2012; Bryukvina et al., 2018). Recent ab-initio calculations

117 (Tiwald et al., 2015; Hoya et al., 2017) have shown that the absorption energy E_a of the F -center
118 (in eV) may be approximated by:

$$119 \quad E_a = 16.5 a^{-1.76} \quad (1)$$

120 where a is the anion-cation distance. Relation (1) gives a physical ground to the classical
121 empirical Mollwo-Ivey relation (Ivey, 1947). The predicted values, 345 and 415 nm, are in good
122 agreement with the experimental values, 328 and 414 nm. In the optical absorption spectrum of
123 villiaumite from Mont Saint Hilaire, Canada (Rossman, 2010), the main absorption band at 510
124 nm shows a slightly different lineshape and additional weak contributions around 400 nm. As in
125 natural blue halite (Zepek et al., 2015), the relative proportion of isolated defect centers and
126 metallic nanoparticles may vary among the samples.

127

128 **Evidence of a plasmon resonance in villiaumite**

129 As indicated above, a Lorentzian lineshape is consistent with a surface plasmon resonance.
130 The position of this resonance is similar to that in synthetic NaF (Chandra and Holcomb, 1969;
131 Bryukvina and Martynovich, 2012; Bryukvina et al., 2018). The resonance wavelength may be
132 predicted from the Mie theory by considering spherical metal particles (Doyle, 1958; Hunault et
133 al., 2017). In this approximation, the average size of the nanoparticles is derived from:

$$134 \quad R = V_f \lambda_p^2 / (2\pi c \Delta\lambda) \quad (2)$$

135 where R is the average radius of the metallic clusters, V_f is the Fermi velocity of the electrons in
136 the bulk metal (for Na, $V_f = 1.07 \times 10^6$ m.s⁻¹), λ_p is the characteristic wavelength at which the
137 surface plasmon resonance (SPR) occurs, $\Delta\lambda$ is the full width at half-maximum and c is the speed
138 of light. This predicts an average diameter of Na nanoparticles slightly smaller than 3 nm. At 10
139 K, this absorption band only slightly shifts by about 10 nm towards higher wavenumbers, without
140 any narrowing. This is consistent with an assignment to a surface plasmon resonance, which does

141 not change in energy or amplitude with temperature, by contrast to the transitions related to color
142 centers (Kreibig and Vollmer, 1995).

143 Color centers in alkali halides have a limited thermal stability above room temperature relative
144 to Na colloids, (Schwartz et al., 2008). This explains why, in the geological samples, a plasmon
145 resonance is predominant over the electronic transitions expected from these color centers.
146 Similar mechanisms have been observed in glasses where alkali ions can act as electron traps
147 upon irradiation and form metal colloids (Boizot et al., 2000). Such processes are thermally
148 activated and demonstrate that alkali ions agglomerate to form bigger complexes after trapping
149 electrons at temperatures reaching a few hundreds °C.

150

151 **Comparison with halite**

152 The shape of the optical absorption spectrum of blue halite from Stassfurt is similar to some of
153 the blue halites above mentioned. It is almost identical to the first absorption spectra published on
154 blue halite (also from Stassfurt: Doyle, 1960) (Supplemental Figure S5). The main absorption
155 band peaks at 640 nm, the same value as reported by previous authors (e.g., Doyle, 1960;
156 Howard and Kerr, 1960). Using several Gaussian-Lorentzian spectral components, assigned to
157 Na colloids and various color centers, gives a good fit (Zelek et al., 2014 and 2015). However,
158 fitting the spectra is non equivocal. Here, we use a minimum number of spectral components, as
159 for villiaumite. The main band, at 640 nm, is fitted with a single Lorentzian component (Fig. 1b),
160 because it arises from a surface plasmon resonance of Na nanoparticles (e.g., Seinen et al., 1994).
161 The FWHM, 105 nm, is similar to the values found in the Klodawa mine (Weselucha-Birczyńska
162 et al., 2012) and larger than in villiaumite (86 nm) . Minor additional Gaussian-shape
163 contributions at 430, 531 and 744 nm may be assigned to *F*-, *R*- (3 neighboring *F*-centers) and *M*
164 (2 neighboring *F*-centers) color centers, respectively. The actual position of these bands is shifted

165 relative to that expected from relation (1), at 473, 550 and 705 nm for the *F*-, *R*- and *M*-centers-,
166 respectively. The same centers are found in the halite from Klodawa mine and a similar
167 discrepancy with the Mollwo-Ivey relation is observed (Weselucha-Birczyńska et al., 2012).
168 Finally, a fourth minor Gaussian contribution occurs at 385 nm as in other natural halites (Doyle,
169 1960; Weselucha-Birczyńska et al., 2012), but its origin is unclear.

170

171 **Scaling the spectra of red villiaumite and blue halite**

172 The halite spectrum presents similarities with that of villiaumite, but occurs at larger
173 wavelengths. As a consequence, the transmission window does not occur in the same spectral
174 region, being located on the long or short wavelength side of the main band in red villiaumite and
175 blue halite, respectively (Figures 1a and 1b). This explains the difference in the color of these
176 minerals, despite both show a broad Lorentzian shape plasmon resonance with spectral properties
177 independent of temperature, which is assigned to the presence of Na nanoparticles. For spherical
178 particles that are smaller than the wavelength of light, the value of the resonance wavelength
179 depends on the refractive index of the surroundings (Kreibig and Vollmer, 1995). The
180 wavelength of maximum absorption λ_{\max} may be predicted within the Mie theory, following the
181 Doyle relation (Doyle, 1958; Davenas et al., 1973; Seifert et al., 1994):

$$182 \lambda_{\max} = \lambda_c (1 + 2n_0^2)^{1/2} \quad (3)$$

183 where n_0 is the refractive index of the host medium and λ_c is the critical wavelength for the onset
184 of ultra-violet transparency of sodium. The ratio between the λ_{\max} values in villiaumite and halite,
185 allows elimination of the λ_c term. The ratio calculated from the refractive index of these minerals
186 is 1.13 to compare to an experimental value of 1.29. This explains qualitatively the redshift of the
187 plasmon band with the increasing refractive index of the mineral. The underestimation of this

188 shift when using relation (3) may come from non-spherical shape effects or size distribution of
189 the Na colloids in geological samples with a complex history relative to laboratory samples...

190

191

IMPLICATIONS

192 The comparison of the optical absorption spectra of halite and villiaumite provides a nice
193 illustration of Mie theory, through the dramatic influence of the refractive index of halides on the
194 energy of the plasmon resonance of the embedded metal nanoparticles. Temperatures up to 300-
195 500°C (Zelek et al., 2015; Weerkamp et al., 1994), crystal dislocations and substituted impurities
196 favor the aggregation of color centers leading to the formation of Na colloids. This explains the
197 predominance of these colloids in natural halides (Seifert et al., 1994), as demonstrated by their
198 bright colors. The formation of Na colloids goes with that of free dihalogen molecules, as in the
199 villiaumite from Kola Peninsula, Russia (Celinski et al., 2016) and can only occur once the
200 crystal cooled down to avoid the annealing of these colloids. It is of interest that natural purple
201 fluorites also owe their color to the presence of Ca nanoparticles. Their optical absorption spectra
202 show an intense, broad absorption band near 560 nm that has been suggested to come from Ca
203 metal colloids (Bill and Calas, 1983; Rossman, 2010; Gaft et al., 2020; Ryskin et al., 2020). The
204 same band is found in additively colored synthetic CaF_2 (Angervaks et al., 2018). This
205 absorption band has a Lorentzian shape, which indicates a plasmon resonance origin (Ryskin et
206 al., 2020). Its position, near 560 nm, is intermediate between that in red villiaumite, 494 nm, and
207 blue halite, 640 nm. This absorption band allows light transmission in both the red and blue
208 regions of the spectrum, resulting in the characteristic purple color of irradiated fluorites. It may
209 be pointed out that the position of the colloid band ranges in the order villiaumite (494 nm)-
210 fluorite (560 nm)-halite (640 nm), i.e. the same ranking as for the refractive indices, 1.3253,
211 1.4338 and 1.5442, hence qualitatively following the prediction of Relation (3).

212 Natural halite exhibits a broad range of colors, navy-blue, blue, purple or colorless arising
213 from various proportions of color centers and Na colloids (Weselucha-Birczynska et al., 2012).
214 Zelek et al. (2014) have shown that this may result from the complex sedimentary geology that
215 governs in the mine the spatial distribution of halite and sylvinite, as ^{40}K is suspected to be the
216 main radiation source. In villiaumite, radiation damage is caused by a specific geological context.
217 Agpaitic rocks are always enriched in Th and U (Sorensen, 1992). Though XRD only indicates
218 the presence of NaF, preliminary SEM-EDS investigations of our samples (Figure 2) show the
219 presence of nanospheres, about 500 nm large, which show a preferential alignment that
220 apparently guides the {100} cleavage steps. These nano-inclusions contain about 8.8wt% ThO_2
221 (Supplemental Figure S6) and may be at the origin of a permanent irradiation of the mineral, able
222 to create defects once the mineral cooled down to a few hundreds °C. This explains the presence
223 of isolated color centers, which otherwise have a limited thermal stability (Schwartz et al., 1994)
224 and the stability of the Na nanoparticles that are at the origin of the red color. The presence of
225 thorium in the villiaumite from the Khibiny and Lovozero alkaline massifs in the Kola Peninsula,
226 Russia (Chukanov et al., 2006) has been explained by its complexation by organic matter, which
227 was revealed by infrared spectroscopy. Preliminary infrared spectra on the villiaumite from the
228 Los Archipelago also reveal the presence of aliphatic hydrocarbon groups and carboxylates in our
229 samples (A. Geisler, unpublished report). The red color of villiaumite, prized in mineral
230 collections, appears to be also a useful "color indicator" of the conditions of emplacement of the
231 evolved stages of peralkaline systems.

232

233

ACKNOWLEDGMENTS

234 We are grateful to Jean-Claude Boulliard for providing the samples and their pictures from the
235 mineral collection of Sorbonne-Université, Maxime Guillaumet for his help on the IMPMC

236 spectroscopy platform and Imene Esteve for the preliminary SEM analyses. We thank Charles
237 Geiger and George Rossman for fruitful suggestions that greatly improved the manuscript.

238

239

REFERENCES CITED

240 Amenu-Kpodo, K., and Neubert, T.J. (1965) Color centers in sodium fluoride. *Journal of*
241 *Physics and Chemistry of Solids*, 26,1615-1619.

242 Angervaks, A.E., Veniaminov, A.V., Stolyarchuk, M.V., Vasilev, V.E., Kudryavtseva, I.,
243 Fedorov, P.P., Ryskin, A.I. (2018) Optical study of calcium precipitates in additively colored
244 CaF₂ crystals. *Journal of the Optical Society of America B*, 35, 1288-1294.

245 Arun, T., Ram, S. S., Karthikeyan, B., Ranjith, P., Ray, D. K., Rout, B., Krishna, J. B. M.,
246 Sengupta, P., and Satyam, P.V. (2017) Ion beam radiation effects on natural halite crystals.
247 *Nuclear Instruments and Methods B*, 409, 216-220.

248 Bill, H., and Calas G. (1978) Color centers, associated rare-earth ions and the origin of
249 coloration in natural fluorites. *Physics and Chemistry of Minerals*, 3, 117-131.

250 Boizot, B., Petite, G., Ghaleb, D. Pellerin, N., Fayon, F., Reynard, B., and Calas, G. (2000)
251 Migration and segregation of sodium under β -irradiation in nuclear glasses. *Nuclear Instruments*
252 *and Methods B*, 166, 500–504.

253 Bryukvina, L., Ivanov, N., and Nebogin, S. (2018) Relationships between lithium and sodium
254 nanoparticles and color centers formation in LiF and NaF crystals with hydroxide and
255 magnesium ions impurities. *Journal of Physics and Chemistry of Solids*, 120,133-139.

256 Bryukvina, L.I., and Martynovich, E.F. (2012) Formation and properties of metallic
257 nanoparticles in lithium and sodium fluorides with radiation-induced color centers. *Physics of the*
258 *Solid State*, 54, 2374-2378.

259 Celinski, V.R., Ditter, M., Kraus F., Fujara F., and Schmedt auf der Günne, J. (2016) Trace
260 determination and pressure estimation of fluorine F₂ caused by irradiation damage in minerals
261 and synthetic fluorides. *Chemistry-A European Journal*, 22,18388–18393.

262 Chan Q. H. S., Zolensky M. E., Kebukawa Y., Fries M., Ito M., Steele A., Rahman Z., Nakato
263 A., Kilcoyne A. L. D., Suga H., Takahashi Y., Takeichi Y., and Mase K. (2018) Organic matter
264 in extraterrestrial water-bearing salt crystals. *Science Advances* 4, eaao3521.

265 Chandra, A., and Holcomb, D.F. (1969) Taxonomy of F-aggregate centers in NaF. *Journal of*
266 *Chemical Physics*, 51, 1509–1523.

267 Chukanov, N.V., Pekov, I.V., Sokolov, S.V., Nekrasov, A.N., Ermolaeva, V.N., and Naumova,
268 I.S. (2006) On the problem of the formation and geochemical role of bituminous matter in
269 pegmatites of the Khibiny and Lovozero alkaline massifs, Kola Peninsula, Russia. *Geochemistry*
270 *International*, 44, 715-728.

271 Davenas, J., Perez, A., Thevenard, P., and Dupuy, C.H.S. (1973) Correlation between
272 absorption bands and implanted alkali ions in LiF. *Physica Status Solidi A*, 19, 679–686

273 Davidson, A.T., Kozakiewicz, A.G., Comins, J.D., and Derry, T.E. (1996) Optical effects in
274 NaF crystals implanted with 100 keV ions. *Nuclear Instruments and Methods B*, 116, 216-219.

275 Doyle, W.T. (1958) Absorption of light by colloids in alkali halide crystals. *Physical Review*,
276 111, 1067-1072.

277 Doyle, W.T. (1960) Coagulation, optical absorption and photoconductivity of colloid centres
278 in alkali halides. *Proceedings of the Physical Society*, 75, 649–663.

279 Gaft, M., Waychunas, G.A., Rossman, G.R., Nagli, L., Panczer, G., Cheskis, D., and Raichlin,
280 Y. (2020) Red photoluminescence and purple color of naturally irradiated fluorite. *Physics and*
281 *Chemistry of Minerals*, 47, 46.

282 Howard, C.L.H., and Kerr, P.F. (1960) Blue halite. *Science*, 132,1886-1887.

283 Hoya, J., Laborde, J.I., Richard, D., and Renteria, M. (2017) Ab initio study of F-centers in
284 alkali halides. *Computational Materials Science*, 139, 1-7.

285 Hunault, M., Loisel, C., Bauchau, F., Lemasson, Q., Pacheco, C., Pichon, C., Moignard, B.,
286 Boulanger, K., Hérold, M., Calas, G., and Pallot-Frossardt, I. (2017) Nondestructive redox
287 quantification reveals glassmaking of rare French gothic stained glasses. *Analytical Chemistry*,
288 89, 6277-6284.

289 Ivey, H.F. (1947) Spectral location of the absorption due to color centers in alkali halide
290 crystals. *Physical Review*, 72, 341–343.

291 Kikuchi, A. and Ozawa K. (1973) Induced F aggregate centres in NaF crystals irradiated with
292 charged particles at low temperature. *Physica Status Solidi A*, 18, 567-578.

293 Kreibitz, U., and Vollmer, M. (1995) Optical properties of metal clusters. Springer:
294 Berlin/Heidelberg.

295 Lacroix, A. (1908) Sur l'existence du fluorure de sodium cristallisé comme élément des
296 syénites néphéliniques des îles de Los. *Comptes Rendus Hebdomadaires des Séances de*
297 *l'Académie des Sciences*, 146, 213-216.

298 Levy, P. W., Loman, J. M., Swyler, K. J., and Klaffty, R. W. (1983) Radiation damage studies
299 on synthetic NaCl crystals and natural rock salt for radioactive waste disposal applications. In:
300 *Scientific Basis for Nuclear Waste Management*, Ed. P.L. Hofman, 136–167.

301 Marks, M.A.W., and Markl, G. (2017) A global review on agpaitic rocks. *Earth-Science*
302 *Reviews*, 173, 229–258.

303 Moreau, C., Ohnenstetter, D., Demaiffe, D., and Robineau, B. (1998) The Los Archipelago
304 nepheline syenite ring-structure: a magmatic marker of the evolution of the Central and
305 Equatorial Atlantic. *Canadian Mineralogist*, 34, 281–299.

306 Okada, T. (2006) Nano-scale particles of mixed alkali-metals in KCl crystals. Journal of the
307 Physical Society of Japan, 75, 094705.

308 Poston, M.J., Carlson, R.W., and Hand, K.P. (2017) Spectral behavior of irradiated sodium
309 chloride crystals under Europa-like conditions. Journal of Geophysical Research, Planets, 122,
310 2644–2654.

311 Przibram K. (1953) Verfärbung und Lumineszenz. Beiträge zur Mineralphysik. Springer-
312 Verlag, Vienna.

313 Rossman G.R. (2010) Mineral spectroscopy server. Caltech. <https://doi.org/10.7907/JYWR->
314 [QQ57](https://doi.org/10.7907/JYWR-QQ57).

315 Ruiz-Fuertes, J., Ibáñez, J., Monteseuro, V., Alencar, I., and Cazorla, C. (2019). Reversible
316 tuning of Ca nanoparticles embedded in a superionic CaF₂ matrix. The Journal of Physical
317 Chemistry C, 123, 19945–19951.

318 Ryskin, A.I., Fedorov, P.P., Lushchik, A., Generalov, M.E., Angervaks, A.E., Stolyarchuk,
319 M.V., Vasil'chenko, E., and Kudryavtseva, I. (2020) Absorption spectrum of dark purple fluorite,
320 Kent deposit, Kazakhstan. Journal of Fluorine Chemistry, 240, 109654.

321 Schwartz, K., Volkov, A.E., Sorokin, M.V., Trautmann, V.C., Voss, K.O., Neumann, R., and
322 Lang, M. (2008) Effect of electronic energy loss and irradiation temperature on color-center
323 creation in LiF and NaCl crystals irradiated with swift heavy ions. Physical Review B, 78,
324 024120.

325 Seifert, N., Ye, H., Tolk, N., Husinsky, W., and Betz G. (1994) The influence of defects and
326 defect clusters on alkali atom desorption stimulated by low energy electron bombardment of
327 alkali halides. Nuclear Instruments and Methods B, 84, 77-88.

328 Selby K., Kresin, V., Masui, J., Vollmer, M., de Heer, W.A., Scheidemann, A., and Knight,
329 W.D. (1991) Photoabsorption spectra of sodium clusters. Physical Review B, 43,4565- 4572.

330 Sonnenfeld, P. (1995) The color of rock salt -a review. *Sedimentary Geology*, 94, 267-276.

331 Sørensen, H. (1992) Agpaitic nepheline syenites—a potential source of rare elements. *Applied*
332 *Geochemistry*, 7, 417-427.

333 Stormer, J.C., and Carmichael, I. (1970) Villiaumite and the occurrence of fluoride minerals in
334 igneous rocks. *American Mineralogist*, 55, 126-134.

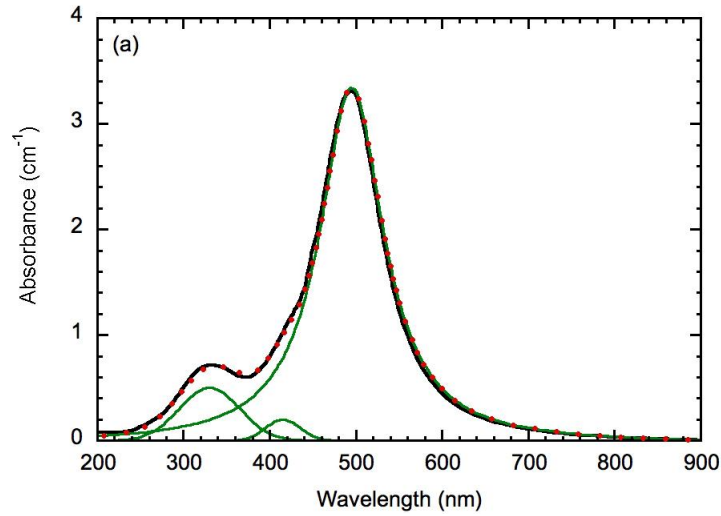
335 Tiwald, P., Karsai, F., Laskowski, R., Gräfe, S., Blaha, P., Burgdörfer, J., and Wirtz, L.
336 (2015) Ab initio perspective on the Mollwo-Ivey relation for F centers in alkali halides. *Physical*
337 *Review B*, 92, 144107.

338 Weerkamp, J.R. W., Groote, J.C., Seinen, J., and Den Hartog, H.W. (1994) Radiation damage
339 in NaCl. I. Optical-absorption experiments on heavily irradiated samples. *Physical Review B*, 50,
340 9781– 9786.

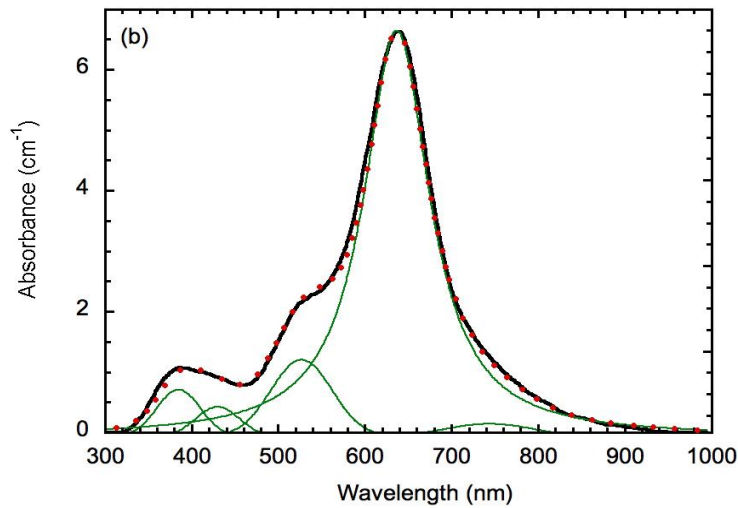
341 Weselucha-Birczynska, A., Zelek, S., and Stadnicka, K. (2012) Blue halite colour centre
342 aggregates studied by micro-Raman spectroscopy and X-ray diffraction. *Vibrational*
343 *Spectroscopy*, 60 124–128.

344 Zelek, S.M., Stadnicka, K.M., Tobola, T., and Nowak, L.N. (2014) Lattice deformation of blue
345 halite from Zechstein evaporate basin: Klodawa Salt Mine, Central Poland. *Mineralogy and*
346 *Petrology*, 108, 619-631.

347 Zelek, S.M., Weselucha-Birczyńska, A., Szklarzewicz, J., and Stadnicka, K.M. (2015)
348 Spectroscopic properties of halite from Klodawa salt mine, Central Poland. *Mineralogy and*
349 *Petrology*, 109, 45–51.



350



351

352

353

354

Figure 1. Room temperature optical absorption spectra of red villiaumite (a) and blue halite (b).

355

These spectra have been background corrected for light scattering by crystal inhomogeneities.

356

The main band, assigned to surface plasmon resonance for metallic Na, shifts by about 140 nm in

357

halite relative to villiaumite. As a consequence, light is transmitted in the long wavelength or

358

short wavelength side of the main absorption band in villiaumite and halite, respectively, hence

359

the spectacular color difference. The fit uses a Lorentzian function for the surface plasmon

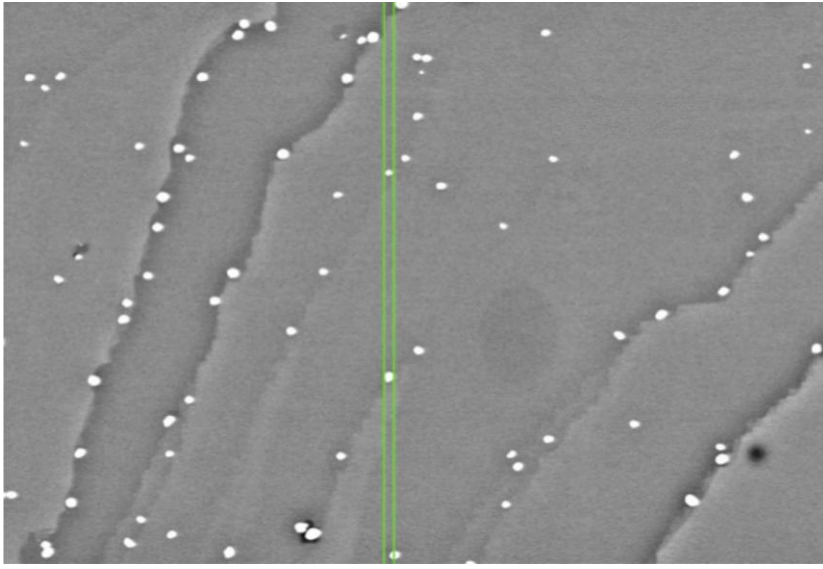
360

resonance (main band) and Gaussian components for the minority transient color centers. The

361

functions used for the fit are displayed in green. The resulting fit gives the red dots.

362



363

364 Figure 2. Scanning Electron Microscopy micrograph in backscattered electron mode of a
365 villiaumite cleavage, showing the presence of thorium-rich nano-inclusions. The scale is given
366 by the green bars, separated by 500 nm. EDS analysis of these nano-inclusions (Supplemental
367 information, Fig. S6) shows that thorium is not accompanied by uranium. The apparent alignment
368 of these inclusions inherits from the growth of the mineral, in which they guide the {100}
369 cleavage steps. These solid inclusions are thought to cause a permanent internal irradiation of the
370 mineral. Once the villiaumite-bearing rock cools down to low temperatures, typically below
371 400°C, this irradiation will progressively cause the formation of radiation-induced color centers
372 and metallic sodium nanoparticles at the origin of the intense red coloration, characteristic of
373 villiaumite.

374